A Mathematical Modeling Framework for Analysis of Functional Clothing

Xiaolin Man[1], Colby C. Swan, Ph.D.[1]

[1]University of Iowa, Iowa City, Iowa USA

Correspondence to:
Colby C. Swan, Ph.D. email: colby-swan@uiowa.edu

ABSTRACT

In the analysis and design of functional clothing systems, it is helpful to quantify the effects of a system on a wearer's physical performance capabilities. Toward this end, a clothing modeling framework for quantifying the mechanical interactions between a given clothing system design and a specific wearer performing defined physical tasks is proposed. The modeling framework consists of three interacting modules: (1) a macroscale fabric mechanics/dynamics model; (2) a collision detection and contact correction module; and (3) a human motion module. In the proposed framework, the macroscopic fabric model is based on a rigorous large deformation continuum-degenerated shell theory representation. Material models that capture the stress-strain behavior of different clothing fabrics are used in the continuum shell framework. The collision and contact module enforces the impenetrability constraint between the fabric and human body and computes the associated contact forces between the two. The human body is represented in the current framework as an assemblage of overlapping ellipsoids that undergo rigid body motions consistent with human motions while performing actions such as walking, running, or jumping. The transient rigid body motions of each ellipsoidal body segment in time are determined using motion capture technology. The integrated modeling framework is then exercised to quantify the resistance that the clothing exerts on the wearer during the specific activities under consideration. Current results from the framework are presented and its intended applications are discussed along with some of the key challenges remaining in clothing system modeling.

INTRODUCTION

Soldiers rely on clothing (a term used herein to include uniforms, body-armor systems, nuclear-biological-chemical war-suits, space suits, etc.) for protection against adversities and threats such as cold weather, ballistic projectiles, radiation, chemicals, and biological agents. While clothing systems provide protection, it has been well established that they can also adversely impact human mobility and comfort in performing physical tasks. For example, if the clothing binds on the wearer's joints, it can restrict motion or make the performance of necessary tasks much more difficult. Alternatively, if the clothing does not permit heat to be conducted or convected away from the body, the wearer can suffer heat-induced fatigue or stroke. A recent study by Rahmatalla et al. (2006) found that the stability of human motion can be significantly affected by clothing restrictions, which eventually causes wearers to change their strategies for accomplishing physical tasks.

The design of functional clothing involves tradeoffs between protection from the adversities noted above and maintained human performance. To facilitate the design process, it is desirable for clothing system designers to have a modeling tool that can realistically evaluate different designs by quantifying the protection they afford and the impact that they have on human performance. To achieve this goal, it is necessary that the clothing be mathematically characterized and modeled in a way that permits interaction with digital human models. In this report, a clothing modeling framework for quantifying the mechanical interactions between a given clothing system design and a specific wearer performing defined physical tasks is proposed and described. The framework consists of three interacting components: (1) fabric mechanics/dynamics modeling; (2) collision detection and contact computation; and (3) digital human modeling. A nonlinear shell theory treatment based on continuum mechanics and dynamics is adopted to represent the fabrics. The collision and contact module enforces the impenetrability constraint between the clothing system and digital human models and computes the mutual contact forces between the two. While the clothing modeling framework will eventually be integrated with intelligent and autonomous digital human models, the human models described in this report are generated by treating the body as a system

of rigid ellipsoids whose dynamic motion is driven by motion capture data. Putting the entire framework together, the clothing is first draped onto the human model's form. Then, as the human form goes through prescribed motions, the contact forces between the draped clothing and the model are computed. The contact forces between the wearer and the clothing are then integrated over space and time to quantify the resistance that the clothing exerts on the wearer during the specific activity considered.

REVIEW

As shear-flexible materials, clothing fabrics develop complex configurations with complicated wrinkling patterns when draped onto objects or the human body. It is a challenge to mathematically model clothing mechanics and to make sense of the apparent disorder in the fabric response to draping. In this section, some key preceding works on fabric modeling are briefly reviewed and classified. The preceding works on mathematical modeling of clothing fabrics essentially break down into two alternative frameworks: (1) particle-based methods in which the fabric is directly discretized into a system of springs and masses; and (2) surface-based methods in which the fabric is treated as an elastic continuum.

Particle-Based Methods

Particle-based methods treat fabrics as a discrete dynamic system composed of mass points or particles that interact through a system of interconnected membrane and bending springs. The coupled equations of motion for all of the "particles" are integrated in time using explicit and implicit algorithms. Simple as they are, such particle methods can generate visually realistic clothing animations and thus have been widely applied in computer graphics and movie-making.

A representative work in particle methods is the mass-spring cloth model proposed in 1995 by Provot (1995) wherein the fabric is modeled as an array of mass particles inter-connected by linear springs of three different types: structural, shear, and flexion (*Figure 1*), which characterize the in-plane stretching, in-plane shear, and out-of-plane bending behaviors, respectively. Structural springs connect a particle with its direct neighbors along two perpendicular axes, which are usually aligned with warp and weft yarn fabric directions, while shear springs connect a particle with its neighbors in the diagonal directions. Flexion springs also act along the two perpendicular yarn axes but each connects every other particle. Cloth drape is solved by an explicit time integration of the system. Since the step size of the integrator is inversely related to the spring stiffnesses, compliant springs were used, which resulted in some unrealistic overstretching of the fabric model. To address this issue, Provot (1995) proposed a heuristic method to adjust particle positions to account for overstretched springs. An extension of the mass-spring model was proposed by Choi and Ko (2002), who considered fabric buckling and included it in the formulation of the bending springs. In their model, a bending spring is treated as a buckling column with both ends pinned, and a nonlinear force-compression relation was derived.

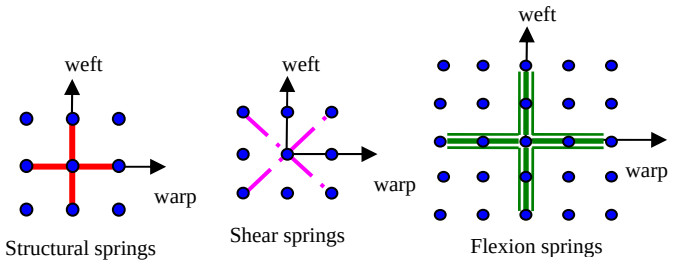

Figure 1. The mass-spring cloth model of Provot (1995).

Breen et al. (1994a, 1994b) incorporated experimental fabric mechanics results into their particle modeling framework that accounts for four different types of mechanical interactions between particles: (1) repulsion, (2) stretching, (3) bending, and (4) in-plane shear. Each type of particle interaction is governed using an independent nonlinear energy function. Draping configurations of fabrics were computed by minimizing the total potential energy of the whole system. The specific energy functions of bending and in-plane shear were based on experimental data obtained from Kawabata Evaluation System for Fabrics (KES-F) (Kawabata, 1980). As the internal forces between particles are computed from the spatial derivatives of the energy functions, the model can be reformulated as a generalized mass-spring model with nonlinear internal forces. The particle-based models of Eberhardt et al. (1996) were similar to those of Breen et al. (1994a, 1994b) with the exception that the internal energy functions were differentiated symbolically, yielding Lagrangian equations of motion for each particle. The resulting differential equations were solved by a Runge-Kutta method with adaptive step-size control. The strain energy functions for bending and in-plane shear were based on experimental data, and fabric hysteresis was included by constructing piecewise linear approximation to experiment curves such as those in *Figure 2*.

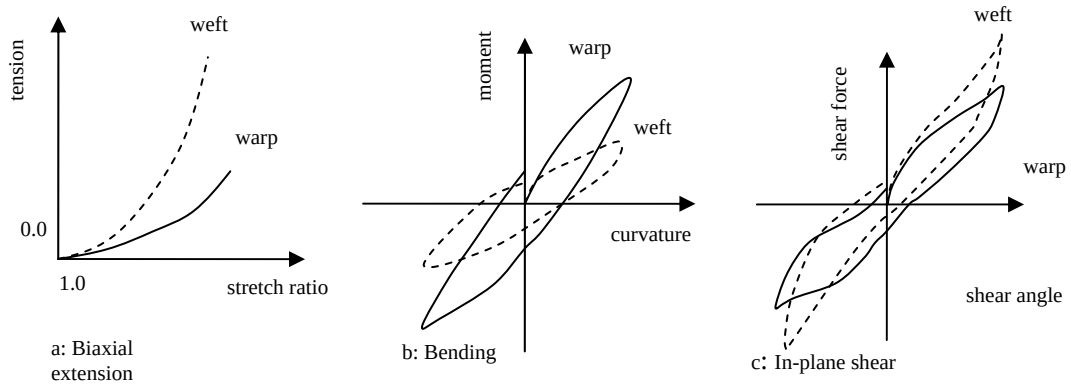

Figure 2. Schematic of different material responses of fabrics.

The particle-based modeling works cited above and numerous other similar works not referenced here are notable for being able to create visually realistic and wrinkled draping configurations of clothing and fabrics. Relatively simple as they are, and yet able to capture the complicated draping configurations of fabrics, particle methods yield helpful insights on issues of fabric modeling. Nevertheless, particle-based modeling of fabrics does have a major shortcoming, and this is that the fabric is directly discretized into a system of lumped masses and springs. In essence, the fabric is treated as a fish-net where the strings and their spacings do not correspond to the yarns that comprise the fabric. As the spatial "fish-net" discretization of a garment is refined, the masses and spring stiffnesses must be adjusted accordingly, and this is not necessarily a trivial matter when dealing with fabric patches of irregular shape and size. The vague physical meaning of spring stiffnesses in particle methods also makes it difficult to translate between fabric spring forces in such models and the actual stress level in the fabric being modeled. Ad-hoc assumptions can and have been made to answer these types of questions, but particle methods lack the rigor of continuum-based methods wherein the relation between forces in the fabric model and fabric stresses and strains is handled both rigorously and straightforwardly.

Continuum Surface-Based Methods

Unlike particle-based methods, surface-based methods take the local equilibrium of a continuum as the point of departure. Models are derived using well established computational techniques, such as approximation of spatial derivatives using finite difference methods, or approximation of the solution space using linearly independent nodal basis functions as in the finite element method. Continuum surface-based methods are generally more rigorous than particle-based methods, both mathematically and mechanically, since the relation between the continuum properties and forces/displacements in the discretized model is based on exact spatial integration. While continuum surface-based methods have a more rigorous foundation than particle-based methods, the implementation of continuum surface-based methods is more involved. Furthermore, since continuum surface-based methods are continuously performing spatial integrations of stresses and strains, such methods are more computationally intensive than particle-based methods, which do not require any spatial integration at all.

While particle-based methods have been more prevalent in mathematical clothing modeling over the past two decades, a number of works have utilized continuum surface methods. To create animations of deformable bodies in computer graphics, Terzopoulos et al. (1987) started with the local form of the Lagrangian equation of motion for a hyperelastic medium, which was then approximated over a regular mesh using finite difference operators. A set of second-order ordinary differential equations was obtained and solved by implicit time integration. This framework was extended by Terzopoulos and Fleischer (1988) to allow for inelastic material behaviors. This framework was later extended by Carignan et al. (1992) for cloth and garment simulation on virtual humans.

In 1991, Collier et al. showed that fabric drape can be predicted using nonlinear shell finite element models. The draping of a circular piece of cotton plain-weave fabric was modeled with 4-node bilinear plate-shell

elements and the results were compared with experimental drape results (Chu et al., 1950; Cusick, 1968). The fabric was modeled first with isotropic and then orthotropic linear elasticity by Collier et al. (1991), and it was discovered that orthotropic elasticity with very high shear compliance is more appropriate for plain-weave fabrics. Three input parameters were needed for the orthotropic model, the tensile moduli in the two yarn family directions, which were measured using KES-F system, and the Poisson's ratio, for which literature values were used. An interesting effect reported was that the computed shape of the draped fabric was sensitive to the Poisson's ratio. A number of similar studies were reported in the mid 1990s by Gan et al. (1995) and by Chen and Govindaraj (1995, 1996), who modeled the fabric with continuum degenerated shell elements. The constitutive relationship used to represent the fabric was orthotropic linear elasticity in which the Young's moduli and the shear moduli were obtained by KES-F and the Poisson's ratio was determined from tensile tests. Chen and Govindaraj (1995, 1996) found that the elastic fabric moduli obtained in the low strain range of Kawabata tests gave realistic drape configurations.

Deviating from continuum degenerated shell elements, Eischen et al. (1996) modeled fabric draping with the geometrically exact resultant shell theory described by Simo and Fox (1989) and Simo et al. (1989, 1990). An isotropic elastic material model with a nonlinear moment/curvature relationship derived from the KES-F system was used. Quasi-static simulations of fabric drape and handling were performed and an arc-length controlled solution technique was utilized to treat instabilities due to fabric buckling. The contact between fabrics and rigid surfaces was considered and the non-penetration constraint enforced by a penalty method.

Since the current work is aimed at accurate and physically realistic modeling of clothing interactions with the human body, the continuum surface approached is adopted for modeling clothing in this effort. As noted previously, such a framework is both mathematically and mechanically rigorous and provides a clear relationship between fabric stress-strain relations and the forces/displacements in the discretized model. If the intent of this work were simply to generate somewhat realistic videos of clothing draped on animated virtual humans, then a particle-based fabric modeling approach would be adopted instead in favor of its relative simplicity and computational efficiency. A continuum degenerated shell approach is taken so that material constitutive models capturing realistic stress-strain behaviors can be employed. A continuum degenerated shell framework is very similar to a three-dimensional continuum mechanics framework in which stress-strain constitutive models are employed with the exception that the special kinematics of a shell are enforced. Alternatively, in resultant shell frameworks [Eischen et al (1996); Simo et al (1989, 1990)] one uses constitutive models in terms of the shell resultants (i.e. moment-curvature relations).

CLOTHING MODELING FRAMEWORK

Fabric Modeling Module

Nonlinear continuum degenerated shell finite element formulation.

The governing continuum equations of motion in a Lagrangian description can be written as follows, using standard continuum mechanics notation (Eringen, 1981):

$$P_{Ji,J} + \rho_0 b_i = \rho_0 \ddot{u}_i \;\forall \mathbf{X} \in \Omega_0 \qquad \textbf{(1)}$$

where Ω_0 is the reference configuration and P_{Ji} is the first Piola-Kirchhoff stress tensor. If tractions $\bar{t}_i^0$ are applied to the system on $\Gamma_{t_i}^0$, then $n_J^0 P_{Ji} = \bar{t}_i^0$ thereon. Furthermore, if prescribed displacements are applied to the system on $\Gamma_{u_i}^0$, then $u_i = \bar{u}_i$ thereon. Introducing a kinematically admissible variational displacement field $\delta\mathbf{u}$ on Ω_0, the weak form corresponding to Eq. (1) is obtained as

$$\int_{\Omega_0} \delta u_{i,J} P_{Ji} \, d\Omega_0 = \int_{\Omega_0} \delta u_i \rho_0 b_i \, d\Omega_0 + \int_{\Gamma_{t_i}^0} \delta u_i \bar{t}_i^0 \, d\Gamma_0 - \int_{\Omega_0} \delta u_i \rho_0 \ddot{u}_i \, d\Omega_0 \qquad \textbf{(2)}$$

The left side of the preceding is the virtual work done by internal stresses, which is denoted as δW^{int}, and it can be verified that

$$\delta W^{int} = \int_{\Omega_0} \delta F_{iJ} P_{Ji} \, d\Omega_0 = \int_{\Omega_0} \tfrac{1}{2} \delta C_{IJ} S_{IJ} \, d\Omega_0 \qquad \textbf{(3)}$$

where $F_{ij} = x_{i,J}$ is the deformation gradient, $C_{IJ} = F_{kI} F_{kJ}$ is the right-Cauchy-Green deformation tensor, and $S_{IJ} = P_{Ik} F_{Jk}^{-1}$ is the 2nd Piola-Kirchhoff stress tensor, which is symmetric.

The geometrical description of a shell, following Hughes (1987), has the initial global position vector

of a material point (ξ,η,ζ) in a shell element that is defined by the following interpolation:

$$\mathbf{X}(\xi,\eta,\zeta)=\sum_{A=1}^{nen}\mathrm{N}_A(\xi,\eta)\overline{\mathbf{X}}_A+\sum_{A=1}^{nen}\mathrm{N}_A(\xi,\eta)\mathrm{z}_A(\zeta)\hat{\mathbf{X}}_A \qquad (4)$$

where in accordance with *Figure 3*, $\overline{\mathbf{X}}_A$ is the initial position vector of node *A*; $\hat{\mathbf{X}}_A$ is the fiber director[1] emanating from node *A* in the fiber direction; $z_A(\zeta)$ is a thickness function; $N_A(\xi,\eta)$ denotes a two-dimensional shape function associated with node *A*; and *nen* is the number of element nodes. At each node, a local fiber coordinate system $(\mathbf{e}^f_{A1},\mathbf{e}^f_{A2},\mathbf{e}^f_{A3})$ is constructed and nodal rotations are specified with respect to the frame. In the initial configuration, $\mathbf{e}^f_{A3}$ is chosen to coincide with the fiber direction $\hat{\mathbf{X}}_A$ and the other two legs are constructed using the algorithm given by Hughes (1987). The updated configuration of the shell is defined in a similar manner as

$$\mathbf{x}(\xi,\eta,\zeta)=\sum_{A=1}^{nen}\mathrm{N}_A(\xi,\eta)\overline{\mathbf{x}}_A+\sum_{A=1}^{nen}\mathrm{N}_A(\xi,\eta)\mathrm{z}_A(\zeta)\hat{\mathbf{x}}_A \qquad (5)$$

where $\overline{\mathbf{x}}_A$ and $\hat{\mathbf{x}}_A$ denote the current nodal position and fiber orientation, respectively.

For finite deformation, these nodal quantities are related to the initial ones as

$$\overline{\mathbf{x}}_A=\overline{\mathbf{X}}_A+\overline{\mathbf{u}}_A \text{ and } \hat{\mathbf{x}}_A=\mathbf{R}\cdot\hat{\mathbf{X}}_A \qquad (6)$$

where $\overline{\mathbf{u}}_A$ denotes the nodal translation and $\mathbf{R}$ is an orthogonal transformation describing a finite rotation of the nodal fiber director. As Eq. (6) suggests, the vector $\hat{\mathbf{x}}_A$ is obtained by rotating $\hat{\mathbf{X}}_A$ by an angle θ about an axis defined by unit vector **n**. According to Euler's theorem, the rotation matrix in Eq. (6) can be written as

$$\mathbf{R}(\boldsymbol{\theta})=\mathbf{I}+\frac{\sin\theta}{\theta}\boldsymbol{\Omega}(\boldsymbol{\theta})+\frac{1-\cos\theta}{\theta^2}\boldsymbol{\Omega}^2(\boldsymbol{\theta}) \qquad (7)$$

with

$$\boldsymbol{\Omega}(\boldsymbol{\theta})=\begin{bmatrix}0&-\theta_3&\theta_2\\ \theta_3&0&-\theta_1\\ -\theta_2&\theta_1&0\end{bmatrix} \text{ and } \theta=(\boldsymbol{\theta}\cdot\boldsymbol{\theta})^{1/2}.$$

In shell kinematics, nodal rotations are permitted about the first two axes of the fiber basis (e.g., $\boldsymbol{\theta}=\theta_{A1}\mathbf{e}^f_{A1}+\theta_{A2}\mathbf{e}^f_{A2}$), which excludes the drilling degree of freedom about $\mathbf{e}^f_{A3}$, and the new orientation of fiber director $\hat{\mathbf{x}}_A$ is thus given by

$$\hat{\mathbf{x}}_A=\hat{\mathbf{X}}_A+\frac{\sin\theta}{\theta}\left(\theta_{A2}\mathbf{e}^f_{A1}-\theta_{A1}\mathbf{e}^f_{A2}\right)+(1-\cos\theta)\mathbf{e}^f_{A3} \qquad (8)$$

The fiber director tip, i.e., $\hat{\mathbf{u}}_A=\hat{\mathbf{x}}_A-\hat{\mathbf{X}}_A$ is

$$\hat{\mathbf{u}}_A=\frac{\sin\theta}{\theta}\left(\theta_{A2}\mathbf{e}^f_{A1}-\theta_{A1}\mathbf{e}^f_{A2}\right)+(1-\cos\theta)\mathbf{e}^f_{A3} \qquad (9)$$

which recovers the infinitesimal rotation case $\hat{\mathbf{u}}_A=\theta_{A2}\mathbf{e}^f_{A1}-\theta_{A1}\mathbf{e}^f_{A2}$ given by Hughes (1987) when $\theta\to 0$.

Considering the shell kinematic relations of Eqs. (4) through (7), the shell configuration is a nonlinear function of nodal translations and rotations, which can be written in abstract form as $\mathbf{x}=\mathbf{x}(\mathbf{d}_A)$ with nodal displacement vector defined as $\mathbf{d}_A=(\overline{u}_{A1},\overline{u}_{A2},\overline{u}_{A3},\theta_{A1},\theta_{A2})^T$. The variation of the updated shell configuration can be written as

$$\delta\mathrm{x}_i=\mathrm{H}^A_{i\chi}\delta\mathrm{d}_{A\chi},(\chi=1,2,\ldots 5) \qquad (10)$$

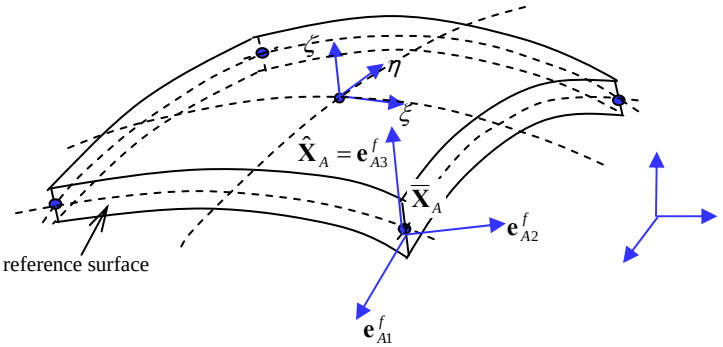

Figure 3. Geometrical description of the shell element

Constitutive model.

In general, woven fabrics are structures of yarns of two families, i.e., warp and weft, woven together following certain weave patterns. Many factors, such

[1] To avoid confusion, the term "fiber director" is standard in shell mechanics and indicates the orientation of a material segment passing through the thickness of the shell. It does not refer to fiber directions in the clothing fabrics being modeled herein. Similarly, the "local fiber coordinate system" is also standard terminology in shell mechanics and does not refer in any way to fiber orientations in the clothing.

as the constituent yarn properties, the weave patterns, the geometry of yarn structures, and the interactions of interwoven yarns, affect the overall material properties of fabrics. As a result, the material properties of fabrics can be extremely complex. Nonlinearity, anisotropy, and hysteresis are generally observed. A typical load-stretch curve of a biaxial extension test of fabrics was shown in *Figure 2a*, which can usually be obtained by Kawabata Evaluation System for Fabrics (KES-F) (Kawabata, 1980). The initial part of the curve is relatively compliant, and it corresponds to yarn decrimping, i.e., the curvatures of yarns decreasing as the yarns are being straightened by tension. Then the fabric shows a much stiffer response as the yarns are actually stretched after they have been straightened. In addition, since the numbers of yarns of the two families and their configurations are usually different, the tensile behaviors of the warp and weft directions differ and exhibit anisotropy. Fabrics also exhibit hysteresis. A load-deformation curve of a fabric bending test is sketched in *Figure 2b*, from which one may notice that energy is dissipated when the fabric is subjected to a loading and unloading loop. Similar behavior can also be observed in the in-plane shear test as shown in *Figure 2c*. The dissipative feature of fabric is due to friction between and within yarns as well as viscoelastic characteristics of the fibers. From *Figure 2c*, one may also notice that fabrics become stiffer when the shear angles increase. This is due to a phenomenon called locking, where yarns jam against each other and further loading induces deformation of yarns' cross sections.

To capture the complex fabric behaviors, mesoscale models with a resolution where yarn interaction is visible are needed, and computational homogenization techniques such as Swan and Kosaka (1997) should be utilized. Currently, research on this multiscale fabric modeling is being actively pursued by the authors. In this work, however, hyperelastic constitutive models, which are based on some simplifying assumptions yet amenable to the shell formulation, are adopted. For hyperelastic materials, a strain energy function $\psi(\mathbf{C})$ exists, and the second Piola-Kirchoff stress tensor $\mathbf{S}$ and the associated tangent elasticity tensor $\mathbf{D}$ can be derived from it as follows:

$$\mathbf{S} = 2\frac{\partial \psi(\mathbf{C})}{\partial \mathbf{C}} \; ; \; \mathbf{D} = 4\frac{\partial^2 \psi}{\partial \mathbf{C} \partial \mathbf{C}} \tag{11}$$

The tangent elasticity tensor $\mathbf{D}$ relates the change of $\mathbf{S}$ to that of $\mathbf{C}$ as $d\mathbf{S} = \frac{1}{2}\mathbf{D} : d\mathbf{C}$. Different definitions of the strain energy function $\psi(\mathbf{C})$ can model materials varying from isotropic elasticity to fiber-reinforced composites (Spencer, 1984). For problems involving large displacements/rotations yet small strains, the St. Venant model provides a good approximation. The model, which is a simple extension of linear elasticity, is as follows:

$$\mathbf{S} = \frac{1}{2}\mathbf{D} : (\mathbf{C} - \mathbf{I}) \tag{12}$$

By assuming that under normal wearing conditions the strains in fabrics are small and linear, the model is used as a placeholder for the constitutive model of the fabric modeling module. The St. Venant model can feature anisotropy and can be easily incorporated in the nonlinear shell formulation.

Most shell theories enforce the so-called vanishing normal stress condition, which requires that the normal stress component acting on a lamina surface vanishes. Enforcing the constraint for general material models can be a nontrivial endeavor (Swan and Cakmak, 1994), so a corotational lamina basis is usually constructed at each quadrature point so that one base vector, say $\mathbf{e}_3^l$, is always orthogonal to the other two, $\mathbf{e}_1^l$ and $\mathbf{e}_2^l$, as the shell deforms, and the Cauchy stress component $\sigma_{33}^l = 0$ is invoked to condense the material tangent moduli (Belytschko et al., 2000; Hughes, 1987). In this work, a similar approach is adopted but is formulated using a Lagrangian description. A lamina basis $\mathbf{E}_I^l, (I = 1, 2, 3)$ is constructed at each quadrature point in the reference configuration, and the vanishing normal stress condition is specified in terms of the 2nd Piola-Kirchhoff stress as $S_{33}^l = 0$, which in general is different from $\sigma_{33}^l = 0$ unless the initial lamina normal remains normal after deformation, i.e., $\mathbf{F} \cdot \mathbf{E}_3^l$ coincides with $\mathbf{e}_3^l$. For thin fabrics, transverse shear is negligible and the condition $S_{33}^l = 0$ closely enforces the vanishing normal stress constraint.

Solution algorithm.

With finite element interpolation in Eq. (5), the weak form of the equation of motion can be transformed into a system of discrete nonlinear equations at a given time $t \in [0, T]$ as

$$\mathbf{r} = \mathbf{f}^{\text{int}} - \mathbf{f}^{\text{ext}} + \mathbf{M} \cdot \mathbf{a} = \mathbf{0}, \tag{13}$$

where $\mathbf{f}^{int}$ and $\mathbf{f}^{ext}$ are the internal and external force vectors, respectively, arising from the left and right sides of Eq. (6) and the term $\mathbf{M}\cdot\mathbf{a}$ is the inertial force vector. Specific expressions for the internal and external force vectors acting on a node A in the model are given as follows:

$$f^{int}_{A\chi} = \int_{\Omega_0} H^{A}_{k\chi,I} F_{kJ} S_{IJ} d\Omega_0$$

and

$$f^{ext}_{A\chi} = \int_{\Omega_0} H^{A}_{i\chi} \rho_0 b_i d\Omega_0 + \int_{\Gamma^0_{t_i}} H^{A}_{i\chi} \bar{t}^0_i d\Gamma_0 \ , (\chi = 1,2,\ldots,5) \qquad \textbf{(14)}$$

For quasi-static problems, the inertial forces can be neglected, although in clothing system modeling, inclusion of such effects tends to increase the robustness of the framework. When clothing is modeled quasi-statically by neglecting inertial terms, buckling and wrinkling instabilities of the fabric create numerical instabilities. Although continuation techniques (Riks, 1972) can help carry the analysis through points of instability, the robustness of the method is still inadequate. Hence, it is generally best to solve the clothing modeling problems as dynamics problems since the mass matrix helps maintain a positive definite tangent operator and stabilizes the system. Newmark's time-integration method (Hughes, 1987) is used to advance the solution in time.

Within the Newmark integration method, both explicit and implicit time integration algorithms can be used with appropriate selection of the two integration parameters. The pros and cons of the implicit and explicit time-integration schemes have been well studied in the literature (Belytschko et al., 2000), so their discussion here is not necessary. However, one observation is that when contact computation is included in fabric modeling, the time step size of an implicit solution scheme may need to be reduced in order to maintain an effective tangent operator, which sometimes makes an explicit integrator a better choice. Such a situation is analogous to automotive crash simulations where explicit solvers dominate.

Collision Detection and Contact Computation Module

This module enforces the impenetrability constraint between clothing and a human model and computes the mutual contact forces between the two. Considering a contact pair designated as a slave node and a master surface segment, the impenetrability constraint requires the slave node not to penetrate the master segment[2]. It is mathematically stated as

$$g = -(\mathbf{x}_s - \tilde{\mathbf{x}}_m)\cdot\mathbf{n} \le 0 \qquad \textbf{(15)}$$

where $\mathbf{x}_s$ is the position of the slave node; $\tilde{\mathbf{x}}_m$ is the closest projection of $\mathbf{x}_s$ onto the master segment; and $\mathbf{n}$ is the outward normal to the master segment at the point $\tilde{\mathbf{x}}_m$. The normal contact traction on the slave node, $\mathbf{t} = t_N \mathbf{n}$, is compressive and the condition is written as

$$t_N \ge 0 \qquad \textbf{(16)}$$

In addition, as the contact pressure vanishes when $g < 0$, the following condition must hold:

$$t_N\, g = 0 \qquad \textbf{(17)}$$

Eqs. (16) through (17) are usually called the Kuhn-Tucker conditions of the impenetrability constraint. The constraint can be enforced by defining the contact pressure as a penalty on the penetration as

$$t_N = \varepsilon_N \langle g \rangle \qquad \textbf{(18)}$$

where $\langle \bullet \rangle = (\bullet + |\bullet|)/2$ is the Macauley bracket function and ε_N is a penalty parameter. The penalty formulation is exact only when $\varepsilon_N \to \infty$. A major problem with the penalty formulation is to choose an appropriate penalty parameter. If the parameter is too small, unacceptable penetration is allowed, and a large penalty parameter can adversely affect the solution procedure. Especially for an explicit solution algorithm, a large penalty significantly reduces the critical step size of the time integrator.

The impenetrability constraint can alternatively be enforced using the Lagrange multiplier method (Carpenter et al., 1991; Belytschko and Neal, 1991), which treats contact tractions as independent variables, namely Lagrange multipliers $t_N = \lambda_N$, and solves the equilibrium simultaneously with Eq. (15). The discrete form of the problem can be written as

[2] Here, the nodes that comprise the clothing model are referred to as "slave nodes" and the polygons that comprise the body surface of the human model are the "master segments."

$$\left.\begin{aligned} \mathbf{f}^{int} + \mathbf{M}\cdot\mathbf{a} + \mathbf{G}^{T}\cdot\boldsymbol{\lambda} &= \mathbf{f}^{ext} \\ \mathbf{G}\cdot\mathbf{x} &= 0 \end{aligned}\right\} \quad (19)$$

where $\boldsymbol{\lambda}$ is a vector collecting all Lagrange multipliers λ_N and $\mathbf{G}$ is a contact constraint matrix, which is derived from Eq. (15) for a given surface discretization. For a master surface segment defined by a quadrilateral as shown in *Figure 4*, the projection point is a bi-linear nodal interpolation as

$$\tilde{\mathbf{x}}_m = \tilde{N}_A \mathbf{x}_{mA}, \quad (A = 1, 2, \ldots 4) \quad (20)$$

where $\tilde{N}_A = N_A(\tilde{\xi}, \tilde{\eta})$ is the shape function evaluated at the natural coordinates of the projection point. The contact constraint matrix associated with the contact pair reads

$$\mathbf{G} = \begin{bmatrix} -1 & 0 & 0 & \tilde{N}_1 & 0 & 0 & \tilde{N}_2 & 0 & 0 & \tilde{N}_3 & 0 & 0 & \tilde{N}_4 & 0 & 0 \\ 0 & -1 & 0 & 0 & \tilde{N}_1 & 0 & 0 & \tilde{N}_2 & 0 & 0 & \tilde{N}_3 & 0 & 0 & \tilde{N}_4 & 0 \\ 0 & 0 & -1 & 0 & 0 & \tilde{N}_1 & 0 & 0 & \tilde{N}_2 & 0 & 0 & \tilde{N}_3 & 0 & 0 & \tilde{N}_4 \end{bmatrix} \quad (21)$$

and the nodal unknowns are

$$\mathbf{x} = \left\{ \mathbf{x}_s^T \quad \mathbf{x}_{m1}^T \quad \mathbf{x}_{m2}^T \quad \mathbf{x}_{m3}^T \quad \mathbf{x}_{m4}^T \right\}^T$$

It can be verified that $\mathbf{G}\cdot\mathbf{x} = -(\mathbf{x}_s - \tilde{\mathbf{x}}_m) = g\mathbf{n}$. Eq. (19b) essentially specifies that the slave node is projected to point $(\tilde{\xi}, \tilde{\eta})$ on the master segment.

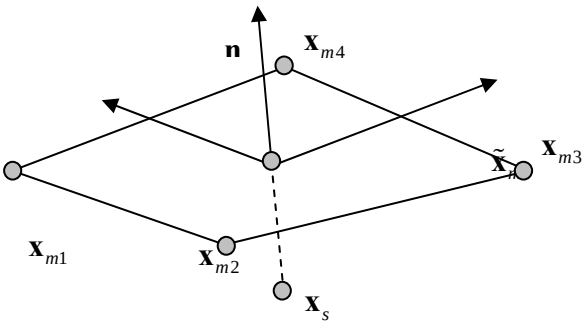

Figure 4. Schematics of impenetrability

Eqs. (19) are solved simultaneously for the deformed configuration and the Lagrange multipliers. For implicit solution methods, as the contact constraint matrix **G** is unknown *a priori*, a trial-and-error procedure is needed to determine the actual active contact constraints. Given a trial configuration, **G** is constructed for penetrating nodes and Eqs. (19) are solved with the trial **G**. If a Lagrange multiplier turns negative, which indicates a tensile traction, the problem is resolved by deactivating the associated constraint. The procedure is iterated until the actual contact surface is determined.

For explicit solution methods, however, the contact surface can be directly determined by the projection of the overlapped volume of the two bodies updated by uncoupled integration, and no iteration is needed. It was shown by Belytschko and Neal (1991) that in this case the Lagrange multipliers are directly determinable and will have the correct sign. A 'forward increment Lagrange multiplier' method was proposed by Carpenter et al. (1991) based on central difference integration. In their approach, a predictor state is first constructed using central difference time integration on both bodies neglecting contact forces, and then the Lagrange multipliers that enforce the impenetrability constraint of the predictor state are solved. Consider a time step from *n* to *n*+1. The equations considered are

$$\left.\begin{aligned} \mathbf{f}^{int}(\mathbf{d}^n) + \mathbf{M}\cdot\mathbf{a}^n + \left[\mathbf{G}(\mathbf{d}^*)\right]^T\cdot\boldsymbol{\lambda} &= \mathbf{f}^{ext} \\ \mathbf{G}(\mathbf{d}^*)\cdot(\mathbf{d}^{n+1} + \mathbf{X}) &= 0 \end{aligned}\right\} \quad (22)$$

where

$$\mathbf{d}^* = (\Delta t)^2 \mathbf{M}^{-1}\cdot\left[\mathbf{f}^{ext} - \mathbf{f}^{int}(\mathbf{d}^n)\right] + 2\mathbf{d}^n - \mathbf{d}^{n-1} \quad (23)$$

is a displacement predictor constructed following standard central difference integration as

$$\mathbf{a}^n = \frac{1}{(\Delta t)^2}(\mathbf{d}^{n+1} - 2\mathbf{d}^n + \mathbf{d}^{n-1})$$

with $\mathbf{a}^n = \mathbf{M}^{-1}\cdot\left[\mathbf{f}^{ext} - \mathbf{f}^{int}(\mathbf{d}^n)\right]$, which excludes the contribution from potential contact forces. A contact constraint matrix is thus constructed based on the predictor state, i.e., $\mathbf{G}(\mathbf{d}^*)$. Assume that a corrector $\mathbf{d}^c$ is introduced such that

$$\mathbf{d}^{n+1} = \mathbf{d}^* + \mathbf{d}^c \text{ with}$$
$$\mathbf{d}^c = (\Delta t)^2 \mathbf{a}^c = -(\Delta t)^2 \mathbf{M}^{-1}\cdot\left[\mathbf{G}(\mathbf{d}^*)\right]^T\cdot\boldsymbol{\lambda}. \quad (24)$$

Eq. (22) yields

$$\boldsymbol{\lambda} = \left[(\Delta t)^2 \mathbf{G}(\mathbf{d}^*)\mathbf{M}^{-1}\mathbf{G}(\mathbf{d}^*)^T\right]^{-1}\mathbf{G}(\mathbf{d}^*)\cdot(\mathbf{d}^* + \mathbf{X}) \quad (25)$$

Substituting Eq. (25) into Eq. (24), the displacement $\mathbf{d}^{n+1}$, which satisfies the impenetrability condition, is obtained.

According to the development presented above, a key component for contact computation is to determine the contact pair, i.e., collision detection. Depending on the geometric representation, the expense of collision detection varies. For a general mesh-to-mesh collision detection, the master segment (polygon) that contains each slave node needs to be identified and the projection point needs to be computed as well. Three sub-problems, namely a global "nearest neighbor" search, a local master segment identification, and a point projection, are involved (Benson and Hallquist, 1990; Hallquist et al., 1985). A brute force search for nearest neighbors has a complexity of $O(N^2)$, provided that each mesh has *N* nodes. If the relative sliding of the contact parts is small, locality can be utilized to reduce the expense by lowering the number of searching candidates. However, such a technique is not applicable to a highly distorted surface, such as a wrinkling cloth, as the locality assumption is broken. In addition, the local search for the master segment containing a given slave node also takes a large amount of computation time. For these reasons, efficient contact detection algorithms still remain a challenging research topic and are being actively pursued, especially in the computer science community. A noticeable work has been reported by Govindaraju et al. (2005), where collision between complex deformable objects can be identified with interactive rates by utilizing special data structures and graphics hardware.

In this work, a collision detection algorithm based on implicit surfaces is adopted for simplicity with the understanding that a more sophisticated and general mesh-to-mesh collision detection component, such as that of Govindaraju et al. (2005), will be substituted in later. An implicit surface $\Im$ is defined as the set of points in three-dimensional space that satisfy a scalar function $f(\mathbf{x}) = 0$. In mathematical terms $\Im = \{\mathbf{x} \in \Re^3 \mid f(\mathbf{x}) = 0\}$. As an example, an ellipsoid with centroid $\mathbf{x}^c$, orientation vectors $\hat{\mathbf{e}}_1, \hat{\mathbf{e}}_2, \hat{\mathbf{e}}_3$, and radii r_1, r_2, r_3 has the implicit surface

$$\Im = \left\{ \mathbf{x} \in \Re^3 \mid f(\mathbf{x}) = \sum_{i=1}^{3} \left\{ \frac{\left[(\mathbf{x} - \mathbf{x}^c) \cdot \hat{\mathbf{e}}_i \right]^2}{r_i^2} \right\} - 1 = 0 \right\} \quad \textbf{(26)}$$

A specific point $\mathbf{y}$ on the clothing model is determined to have penetrated the implicit surface $\Im$ when $f(\mathbf{y}) < 0$. The penetrating point must then be returned to the nearest point on the implicit surface $\Im$. When the human body surface is modeled as an assemblage of ellipsoids (*Figure 5b*), the computational cost for collision detection is minimized. Nevertheless, the ellipsoidal human surface model is only a gross representation and serves as a placeholder for higher-fidelity polygonal surface meshes of the human body (Swan, 2007) that will use efficient mesh-to-mesh collision detection.

To simplify the clothing modeling computations, the ellipsoids are treated as rigid with their motions fully prescribed and thus independent of the clothing interaction. With the body motions fully prescribed the analysis problem is thus reduced to solving for the clothing model's response to a set of captured motions. For each time step of the clothing modeling problem, a kinematic predictor is constructed based on Eq. (23). Eq. (22b) essentially projects a penetrating slave node back onto the master surface. With an ellipsoidal surface, this can be done by finding the intersection of the gradient at the penetrating position with the surface. The corrector displacement $\mathbf{d}^c$ is thus determined and the Lagrange multiplier can then be obtained by inverting Eq. (24). It can also be assumed that since the kinematics description of the ellipsoidal surface is available, the post impact kinematics state of a penetrating slave node can be interpolated from that of the master surface based on non-resilient impact response. The assumption basically specifies that the clothing moves with the human body surface.

Human motion module

The human model is grossly represented by an assemblage of rigid ellipsoids the kinematics of which are driven by human motion capture data. The human motions utilized in Section 4.2 were captured with an eight-camera Vicon® Motion Capture system that collects digital images at a rate of 200 frames per second. The human subject on whom the motion capture is performed wears a black lycra suit with reflective plastic marker beads attached. As the human subject performs a physical activity, the system's cameras collect digital photographs. The processor of the motion capture system then uses the digital images and triangulation to calculate the location of each marker to a precision of approximately 1mm at the instant of each captured frame. From the locations of the markers, the location time histories of joint centers (knees, hips, angles, etc) are then constructed.

As each ellipsoid is treated as a rigid entity, the space it occupies at any instant in time is determined by the location of the centroid as well as the orientation and radii of the ellipsoid. This information is obtained from the location history of two joint centers that are diametrically opposed points $\mathbf{J}_1$ and $\mathbf{J}_2$, and the location history of an auxiliary marker position **M** (*Fig. 5a*). The centroid and the orientation basis of the ellipsoid at any instant in time are then constructed as follows:

$$\text{centroid: } \mathbf{x}^c = \frac{1}{2}(\mathbf{J}_1 + \mathbf{J}_2) \qquad \textbf{(27a)}$$

$$\text{orientation: } \hat{\mathbf{e}}_1 = \frac{\mathbf{J}_2 - \mathbf{J}_1}{\|\mathbf{J}_2 - \mathbf{J}_1\|};\ \hat{\mathbf{e}}_2 = \frac{(\mathbf{M} - \mathbf{x}^c) - [(\mathbf{M} - \mathbf{x}^c)\cdot\hat{\mathbf{e}}_1]\hat{\mathbf{e}}_1}{\|(\mathbf{M} - \mathbf{x}^c) - [(\mathbf{M} - \mathbf{x}^c)\cdot\hat{\mathbf{e}}_1]\hat{\mathbf{e}}_1\|};\ \hat{\mathbf{e}}_3 = \hat{\mathbf{e}}_1 \times \hat{\mathbf{e}}_2 \quad \textbf{(27b)}$$

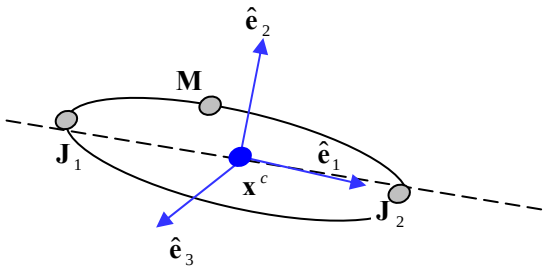

(a) re-constructing the motion of each ellipsoid using motion capture data that records for each ellipsoid the position histories of points $\mathbf{J}_1$, $\mathbf{J}_2$, and **M**

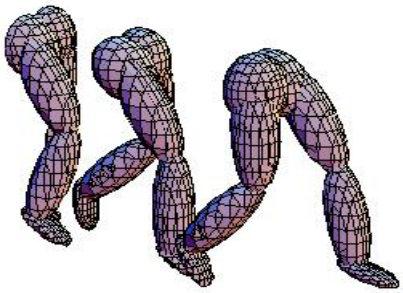

(b) a lower-body walking model

Figure 5. Representation of the human body with an assemblage of rigidly translating, rotating, and overlapping ellipsoids

RESULTS

Based on the proposed computational framework, the mechanical interactions between clothing and a wearer can be quantified. A general procedure is as follows: Given wearer's motions, the contact tractions between clothing and human body surfaces are solved and the stresses and the strains in clothing fabrics are determined as well. These mechanical quantities are then related to certain predefined restriction measures, such as joint torque or energy expenditure, to quantify the effect of clothing on the wearer for the given motion. Currently the motion is prescribed and is assumed to be independent of the clothing restrictions.

In the following section, some examples are presented to illustrate the methodology. The restriction measure adopted here is the torque exerted by clothing on a given joint. It is computed as follows.

$$\boldsymbol{\tau} = \sum_{i \in AJ} (\mathbf{x}_i - \mathbf{J}) \times \boldsymbol{\lambda}_i \qquad \textbf{(28)}$$

where $\mathbf{x}_i$ is the position of a clothing node; $\boldsymbol{\lambda}_i$ is the nodal contact force vector acting on the human body; **J** denotes the instantaneous coordinates of the joint center; and *AJ* is the set of nodes that contribute to the torque on the joint **J** under consideration. The composition of *AJ* needs further study to determine which portions of the clothing exert meaningful torque on each joint. A schematic about the joint torque computation is given in *Figure 6.*

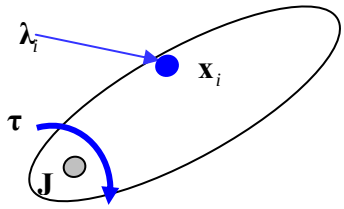

Figure 6. Computation of torques exerted by the clothing about the joint centers

Arm-Sleeve Interaction Study

In this example, the interaction between an arm represented by two rigid ellipsoids and a cotton sleeve is studied. The forearm ellipsoid has radii ($r_1 = r_2 = 0.06\text{m}, r_3 = 0.20\text{m}$) while the upper arm ellipsoid has radii ($r_1 = r_2 = 0.06\text{m}, r_3 = 0.15\text{m}$). The motion considered is to flex the forearm about the elbow joint while keeping the upper arm fixed. The torque exerted by the sleeve about the elbow joint is calculated. The sleeve is modeled as a cylindrical tube with length $L = 0.5m$, radius $R = 0.06m$, and thickness $t = 1mm$. Boundary conditions are specified to restrain the motion of fabric nodes around the shoulder. The upper- and fore-arms are modeled as two ellipsoids, one fixed in space and the other rotating about the elbow joint with a constant

angular velocity. The total rotation angle is 57° before severe clothing self-contact occurs and the computations are stopped.

A plain-weave cotton fabric at low tensile stresses (less than 1 MPa) tends to have a very small Young's modulus due to the crimp in the yarns and is denoted here as "crimped cotton." At higher tensile stresses as the yarns become taut, the Young's modulus of the fabric increases dramatically and approaches the product of the cotton fiber modulus (7.9 GPa) and the volume fraction of fibers running in the direction of interest. When modeling crimped cotton fabric a very low Young's modulus $E = 1.2\,MPa$ is employed in the warp and weft directions, while a low shear modulus $G=0.1\ MPa$ is selected to capture the high shear compliance of the fabric. If it is assumed that the cotton fiber volume fraction in the fabric is roughly 30 %, then a suitable approximation for the mass density of the fabric would be 30% that of cotton fibers. Accordingly a nominal mass density of the plain-weave cotton fabric has been selected as 436 kg/m^3. For plain-weave cotton at stresses above about 10 MPa, the yarns become taut and we refer to the fabric as "de-crimped." A representative Young's modulus of 350 MPa is employed in the warp and weft directions for de-crimped cotton, which is roughly 4.4% of the fiber modulus. The shear stiffness and mass density of the fabric are assumed to remain unchanged.

To model friction between the clothing and the body, simple Coulomb friction with a constant coefficient of friction μ is employed. It is acknowledged that such a treatment of friction is highly simplistic and only begins to capture the rich complexity of frictional interactions that occur between clothing and the human body surface. Due to the uncertainty in the coefficient of friction between clothing and skin of the body, values within the range of $\mu \in [0.1, 0.5]$ are employed in this study.

Convergence study.

The convergence behavior of the model in terms of mesh refinement is investigated. Four models of crimped cotton sleeves and friction coefficient $\mu = 0.1$ with varying mesh densities (*Figure 7*) are constructed and then resistance torque versus rotation angle curves are computed (*Figure 8*). It is found that the curves deviate slightly but follow a similar trend of reduced resistance with increasing refinement. A comparison of the computed deformations (*Figure 9*) shows that finer meshes capture local fabric buckling (wrinkling), which may not occur on the coarser meshes. The finding of increasing localized fabric wrinkling with increasing mesh refinement indicates potential instability of the system. The same convergence study was conducted with a higher friction coefficient $\mu = 0.5$, and a more defined convergence behavior of the resistance torque is observed (*Figure 10*). As shown in the deformed configurations (*Figure 11*), higher friction between the arm and the sleeve prevents the sleeve from falling down onto the elbow joint and thus reduces the amount of wrinkling that occurs at the elbow. Comparison of *Figures 8* and *10* indicates that clothing resistance torques increase very significantly with higher friction between the arm and sleeve.

Friction.

The friction between clothing and human body surface is an important factor affecting the interaction of the two. For a crimped cotton sleeve model with a well-refined mesh, the low friction case ($\mu = 0.1$) is compared with a high friction case ($\mu = 0.5$). It is found once again that in the low friction case the sleeve slips down as the forearm rotates upward. Alternatively, in the high friction case, the sleeve does not slide down the forearm. Snapshots of the sleeve deformation for both the low and high friction cases are shown in *Figure 13* at two elbow flexion angles, $\alpha = 37^\circ$ and $\alpha = 57^\circ$. It is noted once again that higher friction between the arm and sleeve translates to higher clothing resistance torque as indicated in *Figure 13*.

Effect of Fit.

To briefly study the effect of clothing fit on resistance, the radius of the sleeve tube is increased from *R=0.06m* to $R = 0.07m$ while the dimensions of the ellipsoidal arms remain the same. The computed resisting torque exerted by the looser-fitting sleeve (*Figure 15*) is significantly less than that of the tighter-fitting sleeve for elbow flexion angles greater than 20°.

Effect of Fabric Thickness.

Fabric thickness is another factor that can affect clothing-wearer interaction. A thicker fabric has greater mass and larger stiffnesses. Membrane stiffnesses increase in proportion to the fabric thickness, while the bending stiffnesses increase in proportion to the thickness cubed. Here, the thickness of the sleeve fabric is doubled to $t = 2\,mm$ and the joint torque is compared with the original case where $t = 1\,mm$. All other properties remain the same, and a surface friction coefficient μ =0.5 is assumed. The computed torque resistance of the thicker fabric is roughly double that of the thinner

fabric, which indicates that membrane rather than bending behavior of the sleeve is dominant.

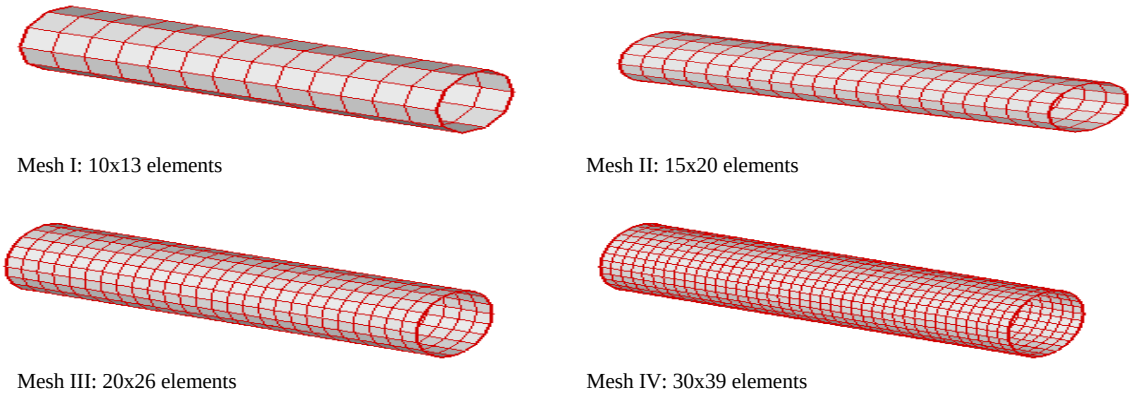

Figure 7. Sleeve models of increasing mesh refinement for convergence study

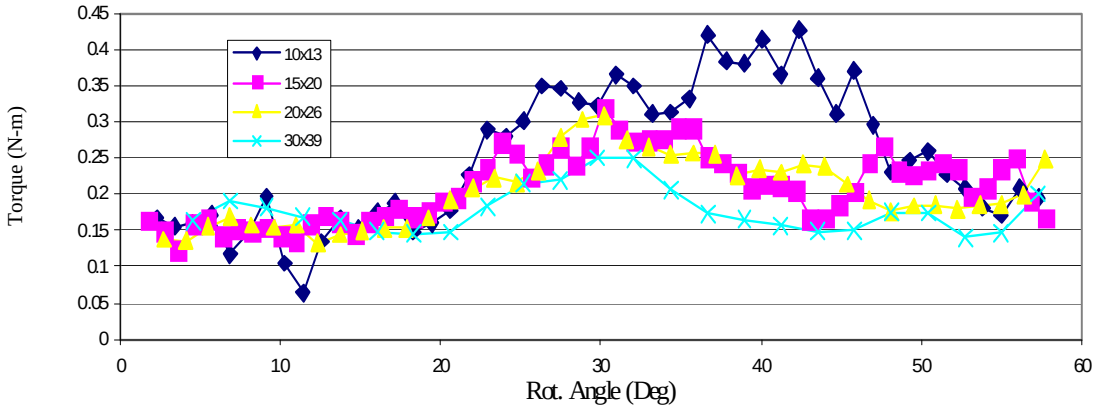

Figure 8. Computed clothing resistance torques about the elbow joint for a crimped cotton sleeve with varying mesh refinement; the Coulomb friction coefficient between arm and sleeve was $\mu = 0.1$.

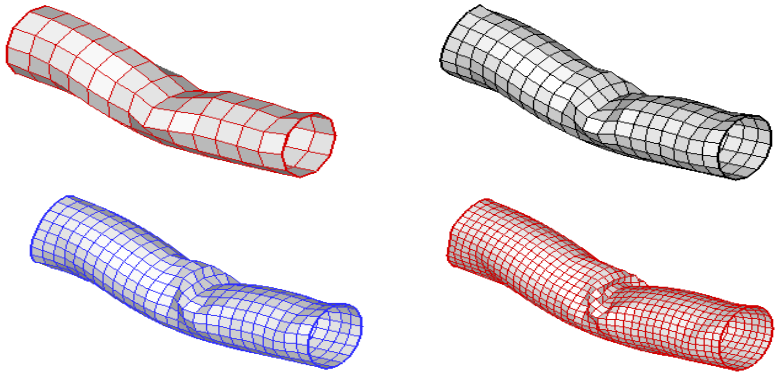

Figure 9. Illustration of localized clothing wrinkling in the elbow joint with increasing mesh refinement (Low Friction $\mu = 0.1$); meshes are shown at elbow flexion angle α=37°

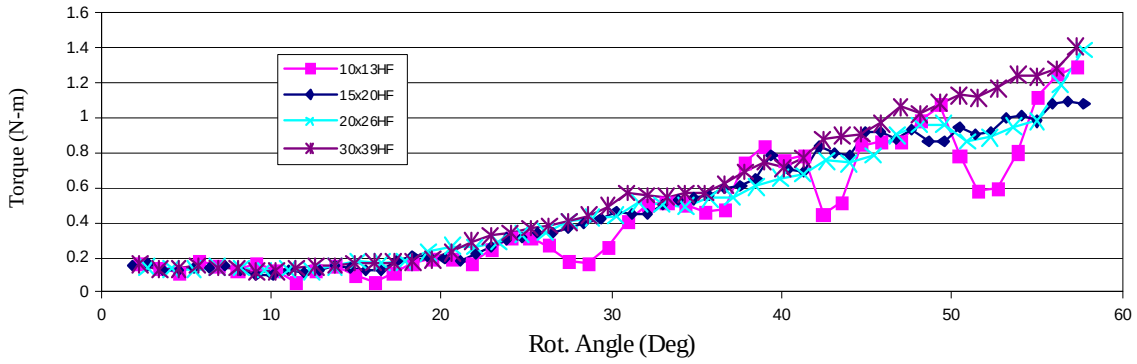

Figure 10. Computed clothing resistance torques about the elbow joint for a crimped cotton sleeve with varying mesh refinement; Coulomb friction coefficient between arm and sleeve was $\mu = 0.5$

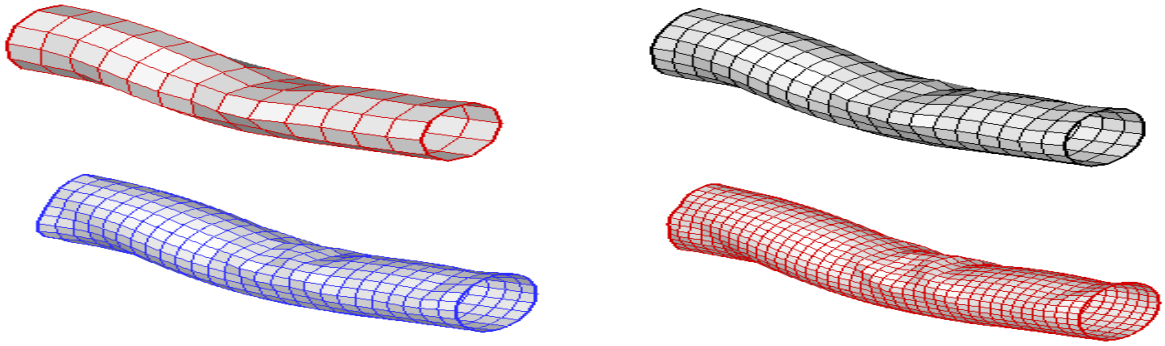

Figure 11. Local buckling is less sensitive to mesh refinement for higher arm-sleeve friction coefficient $\mu = 0.5$. Meshes are shown at elbow flexion angle α=37°.

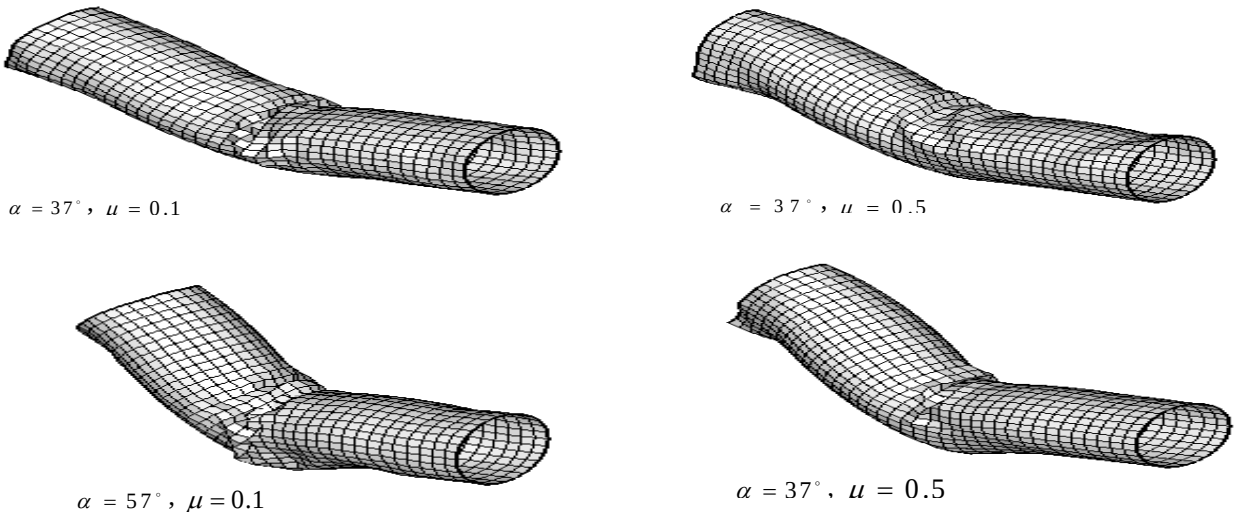

Figure 12. Sleeve deformations for crimped cotton fabric and different friction coefficients

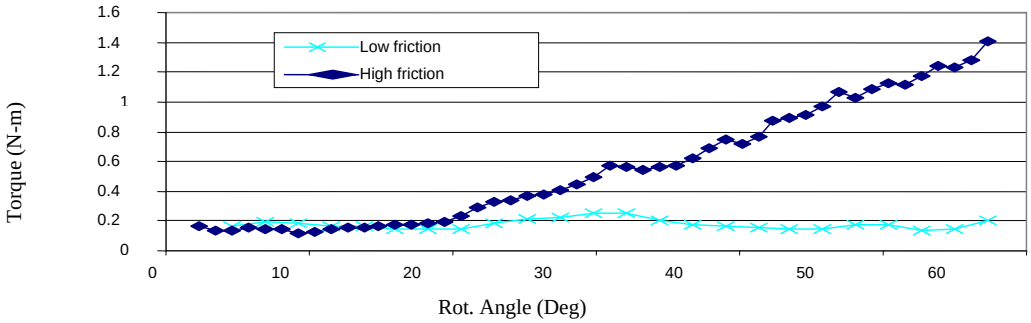

Figure 13. Clothing joint resistance torque exerted for different surface friction coefficients

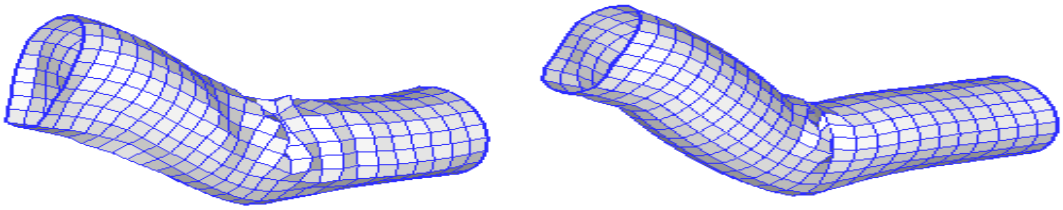

Loose fit: R=0.07m Tight fit: R=0.06m

Figure 14. Deformed configurations of sleeves with different sleeve radii.

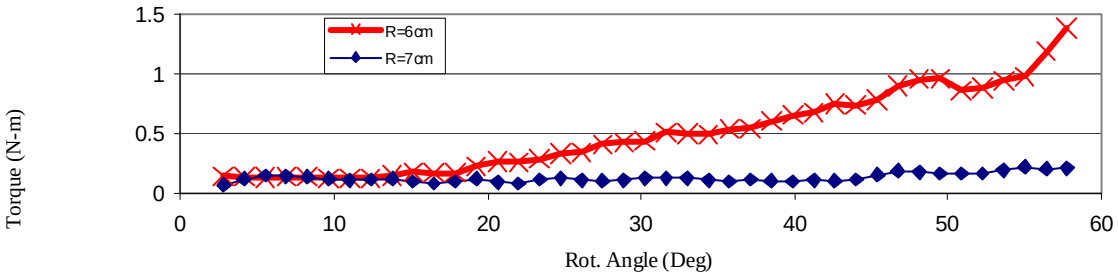

Figure 15. Computed resisting torques exerted by sleeves with different radii; the sleeve is compliant crimped cotton, and the skin friction coefficient is μ=0.5

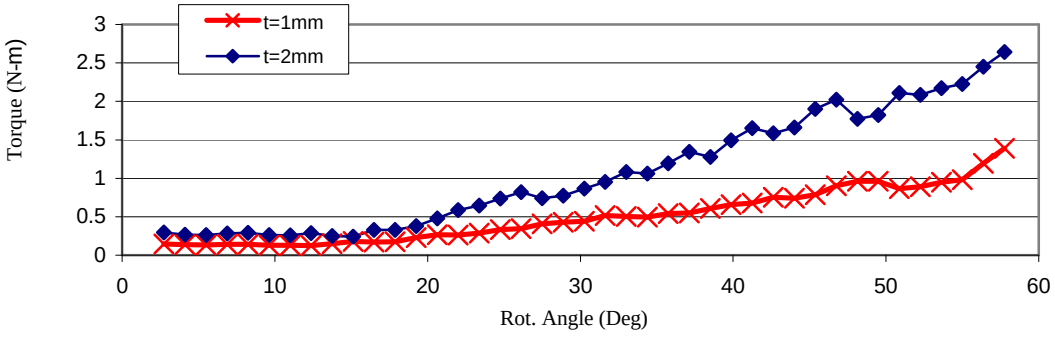

Figure 16. Comparison of crimped cotton sleeve torque resistances with different fabric thicknesses.

Effect of Fabric Material Properties.

The last variation of the arm-sleeve problem examined here focuses on the effect of fabric material properties. Three sets of material properties are examined, roughly corresponding to (I) a crimped cotton sleeve of thickness 1mm; (II) a taut de-crimped cotton fabric of thickness 1mm; and (III) a de-crimped plain-weave Kevlar fabric of thickness 1mm.

Set I: $E = 1.2MPa$ and $\rho = 436Kg/m^3$;
Set II: $E = 350MPa$ and $\rho = 436Kg/m^3$;
Set III: $E = 7.2GPa$ and $\rho = 700Kg/m^3$.

The shear compliance of fabrics significantly affects their drapeability. For all of the three material assumptions considered here, the shear stiffness of the fabric in each case is taken as $1/200^{th}$ of the Young's modulus in the yarn directions. Low surface friction $\mu = 0.1$ is assumed for all of the computations. The computed resistance torques for the three different sleeve materials are presented in *Figure 17*. A stiff response is observed for both material sets II and III, and then a compliant response follows after the rotation angle reaches about 15°. By tracking the deformation of the sleeve, it is found that before reaching an elbow flexion angle $\alpha = 15^\circ$ the sleeve response is governed by bending; after that, the sleeve literally slides down along the forearm. As would be expected, it is also observed that the resistance torque exerted by each sleeve is roughly proportional to the stiffness of the material.

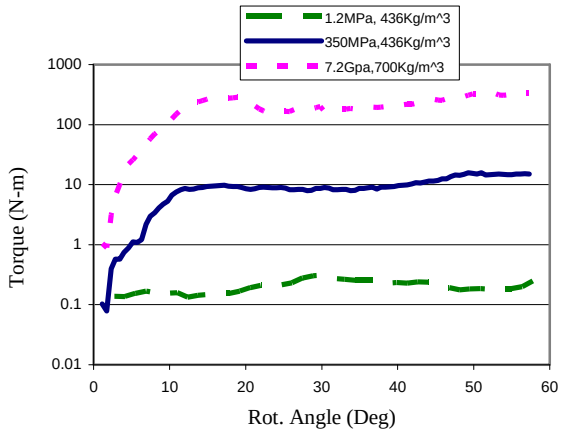

Figure 17. Comparison of sleeve torque resistance for types of fabrics.

Interaction of Pants with Walking/Stepping Legs

In this problem, a human subject walked four strides, with the third involving stepping over an obstacle 0.5m in height. The motion of this human was captured with an array of eight infrared VICON cameras, and the motions were then mapped onto the assemblage of ellipsoids (*Figure 5b*) to make them walk. A pair of pants was then placed onto the human model (*Figure 18*) in the following sequence: (a) the feet of the human model were removed; (b) the pants of the human model were pulled up over the legs and pelvis; (c) the feet of the human model were then restored; and (d) the effect of a belt was created by tensioning the fabric at the waistline. With the garment on the human model, a simulation of the interaction between the pants and the lower body walking and crossing the obstacle was then undertaken (*Figure 19*). Two sets of pants were modeled, both made of compliant, crimped cotton. The first pair had a thickness of 1mm while the second had a thickness of 2mm.

The resistance that the pants models exert on the legs as they undergo their fully prescribed motions was calculated by taking the contact forces exerted by the clothing on the legs at each instant of the simulations and computing their instantaneous moment magnitude about the knees. Such computations are shown in *Figure 20* for two pairs of cotton pants which are identical except for the fabric thickness. Not surprisingly, the thicker pants exert greater resistance torques than do the pants with the thinner fabric. The computed torques about the right knee are due strictly to the pants at the knee level and below. Contributions of the upper pant legs to the resistance have been neglected here. Videos of these "walking pants" simulations are available at Swan (2007).

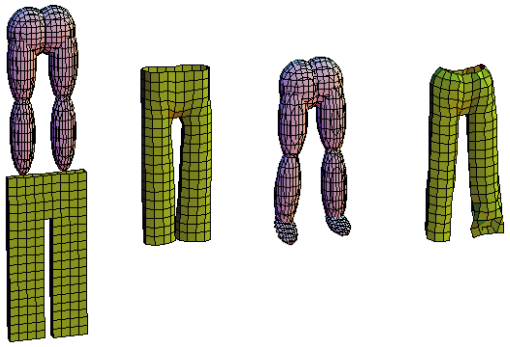

Figure 18. Sequence for the human model to don a pair of pants.

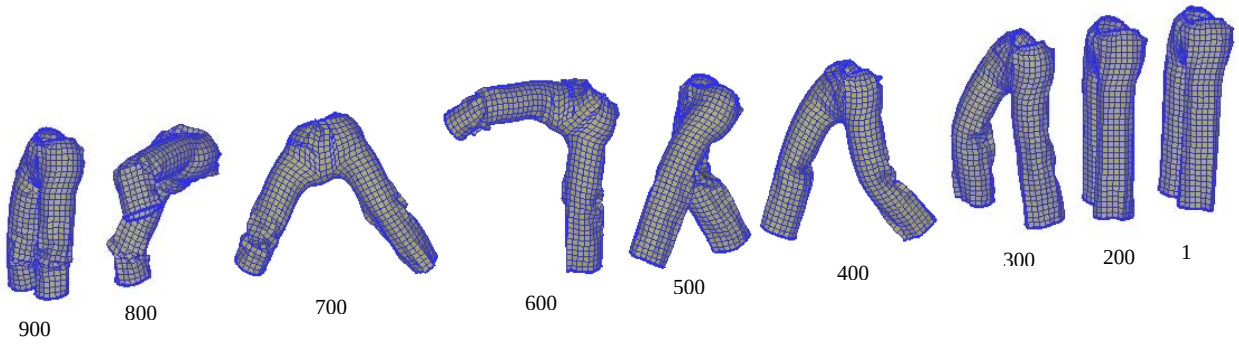

Figure 19. Simulation of pants interacting with lower body striding and then stepping over an obstacle. Numbers below each figure indicate the frame number of the simulation (c.f. Fig. 20)

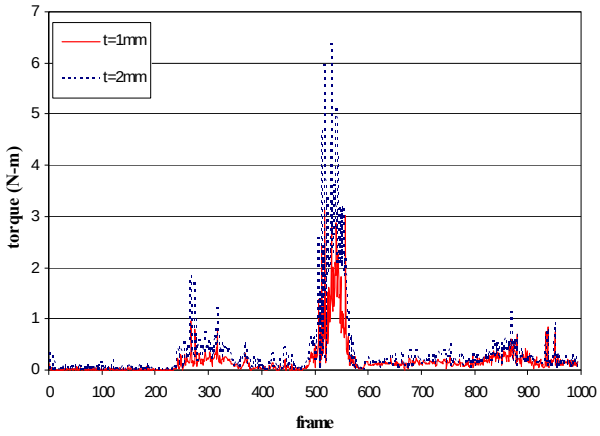

Figure 20. Computed resistance torques exerted by two pairs of cotton pants of different fabric thicknesses about the right knee

DISCUSSION and CONCLUSIONS

A modeling framework has been presented for quantifying the resistance a given clothing system design will exert on a human model of a specified anthropometry performing a specific task, with the associated kinematics measured via motion capture. In the current framework, the anthropometry of the human is modeled rather approximately using rigid ellipsoidal segments. Usage of more realistic polygonal body-surface models (Swan, 2007) based on laser body scans of human subjects can and will be used in subsequent applications of this framework.

In the current examples, the motion of the human model is fully prescribed. It is realized that if the clothing system exerts significant resistance on the wearer tasked to perform a certain task, the wearer might actually change the strategy for accomplishing the task to reduce clothing resistance. Although such effects are not captured in the current framework, this is one of the key objectives of our research effort: to develop autonomous digital human models that can indeed adapt to the resistance they experience.

Two alternative macroscale fabric modeling techniques have been implemented and tested in our clothing modeling framework: The first is a particle-based method that begins with a discrete treatment of the fabric as a system of springs and masses. By experimenting with the spring stiffnesses and masses in such a modeling framework, simulations of clothing that appear visually realistic can be achieved. However, if the objective of the modeling is to realistically quantify the mechanical resistance that the clothing exerts on the wearer, visual realism alone will not be sufficient. For this reason, the continuum degenerated shell formulation implemented and tested in the current framework is somewhat more attractive to the authors. Specifically, one can insert realistic constitutive material models for fabrics and/or body armor segments into the continuum shell framework, thereby increasing the likelihood of calculating more realistic mechanical resistance parameters. Indeed, mechanical realism is paramount in a clothing modeling framework used in designing protective systems for defense and security applications. Due to the relative simplicity of the spring-mass particle method used herein, it might be especially useful to get the clothing system properly positioned on or donned by the digital human model. However, when the real activity of vital interest is performed, the framework can then switch over to the more realistic continuum shell treatment of the clothing.

The results presented herein are intended to be demonstrative rather than definitive in nature to illustrate the nature of the clothing modeling framework. In the current framework, clothing forces and torques exerted on a human model can be

quantified for different fabric types and garment fits. It follows that standard measures of clothing resistance, which can be computed within mathematical modeling frameworks such as that presented here, should be given careful consideration. Clearly, the net mechanical energy dissipated by clothing would be one good measure, but other measures could also be helpful.

Within a mathematical modeling framework for functional clothing, one of the key challenges that remains to be addressed in a satisfactory manner is that of realistically modeling the fabric response characteristics in a way that captures the nonlinearity, anisotropy, and mechanical hysteresis of most functional clothing fabrics.

ACKNOWLEDGEMENT

This work was funded in part by research grants by the U.S. Army TACOM and by the U.S. Army Natick Soldier Center. The authors also express their gratitude to Dr. Salam F. Rahmatalla for his invaluable work in capturing the motion of the walking/striding legs.

REFERENCES

[1] Bathe, K.J. (1982). *Finite Element Procedures in Engineering Analysis*, Prentice-Hall, Englewood Cliffs, NJ.

[2] Belytschko, T., Liu, W.K. and Moran, B. (2000). *Nonlinear Finite Elements for Continua and Structures*, John Wiley & Sons, Ltd.

[3] Benson, D.J. and Hallquist, J.O. (1990). "A single surface contact algorithm for the post-buckling analysis of shell structures," *Computer Methods in Applied Mechanics and Engineering*, 78: 141-163.

[4] Breen, D.E., House, D.H. and Wozny, M.J. (1994a). "A particle-based model for simulating the draping behavior of woven cloth," *Textile Research Journal*, 64(11): 663-685.

[5] Breen, D.E., House, D.H. and Wozny, M.J. (1994b). "Predicting the drape of woven cloth using interacting particles," *Computer Graphics* (*Proc. SIGGRAPH*), 365-372.

[6] Carignan, M., Yang, Y., Thalmann, N.M. and Thalman, D. (1992). "Dressing animated synthetic actors with complex deformable clothes," *Computer Graphics*, 26(2): 99-104.

[7] Chen, B. and Govindaraj, M. (1995). "A physically based model of fabric drape using flexible shell theory," *Textile Research Journal*, 65(6): 324-330.

[8] Chen, B. and Govindaraj, M. (1996). "A parametric study of fabric drape," *Textile Research Journal*, 66(1): 17-24.

[9] Choi, K. and Ko, H. (2002). "Stable but responsive cloth," In *Computer Graphics* (*Proc. SIGGRAPH*), 604-611.

[10] Chu, G.C., Cummings, C.L. and Teixeira, N.A. (1950). "Mechanics of elastic performance of textile materials, Part V: A study of the factors affecting the drape of fabrics – The development of a drape meter," *Textile Research Journal*, 20: 539-548.

[11] Collier, J.R., Collier, B.I., O'Toole, G. and Sargand, S.M. (1991). "Drape prediction by means of finite-element analysis," *Journal of the Textile Institute*, 82(1): 96-107.

[12] Cusick, G.E. (1968). "The measurement of fabric drape," *Journal of the Textile Institute*, 59(6): 253-260.

[13] Eberhardt, B., Weber, A. and Strasser, W. (1996). "A fast, flexible, particle-system model for cloth draping," *IEEE Computer Graphics and Applications*, 16(5): 52-59.

[14] Eischen, J.W. Deng, S. and Clapp, T.G. (1996). "Finite-element modeling and control of flexible fabric parts," *IEEE Computer Graphics and Applications*, 16(5): 71-80.

[15] Eringen, A.C.E. (1981). *Mechanics of continua*, Krieger.

[16] Gan, L., Ly, N.G. and Steven, G.P. (1995). "A study of fabric deformation using nonlinear finite elements," *Textile Research Journal*, 65(11): 660-668.

[17] Govindaraju, N.K., Knott, D., Jain, N., Kabul, I., Tamstorf, R., Gayle, R., Lin, M.C. and Manocha, D. (2005). "Interactive collision detection between deformable models using chromatic decomposition," *Proc. of ACM SIGGRAPH*, 24(3): 991-999.

[18] Hallquist, J.O., Goudreau, G.L. and Benson, D.J. (1985). "Sliding interfaces with contact-impact in large-scale Lagrangian computations," *Computer Methods in*

Applied Mechanics and Engineering, 51: 107-137.

[19] Hughes, T.J.R. *The Finite Element Method Linear Static and Dynamic Finite Element Analysis*, Prentice-Hall, Inc., Eaglewood Cliffs, NJ, 1987.

[20] Kawabata, S. (1980). *The Standardization and Analysis of Hand Evaluation* (The Textile Machinery Society of Japan, Osaka.

[21] Laursen, T.A. and Simo, J.C. (1993). "A continuum-based finite element formulation for the implicit solution of multibody, large deformation frictional contact problems," *International Journal for Numerical Methods in Engineering*, 36: 3451-3485.

[22] Provot, X. (1995). "Deformation constraints in a mass-spring model to describe rigid cloth behavior," *Proc. Graphics Interface*, 147-154.

[23] Rahmatalla, S., Kim, H., Shanahan, M. and Swan, C.C. (2006). "Effect of restrictive clothing on balance and gait using motion capture and dynamic analysis," Paper# 2005-01-2688, *SAE 2005 Transactions Journal of Passenger Cars-Electronic and Electrical Systems*.

[24] Riks, E. (1972). "The application of Newton's method to the problem of elastic stability," *Journal of Applied Mechanics*, 39:1060-1065.

[25] Simo, J.C. and Fox, D.D. (1989). "On a stress resultant geometrically exact shell model. Part I: Formulation and optimal parameterization," *Computer Methods in Applied Mechanics and Engineering*, 72: 267-304.

[26] Simo, J.C., Fox, D.D. and Rifai, M.S. (1989). "On a stress resultant geometrically exact shell model. Part II: The linear theory; computational aspects," *Computer Methods in Applied Mechanics and Engineering*, 73: 53-92.

[27] Simo, J.C., Fox, D.D. and Rifai, M.S. (1990). "On a stress resultant geometrically exact shell model. Part III: Computational aspects of the nonlinear theory," *Computer Methods in Applied Mechanics and Engineering*, 79: 21-70.

[28] Simo, J.C. and Laursen, J.C. (1992). "An augmented Lagrangian treatment of contact problems involving friction," *Computers and Structures*, 42: 97-116.

[29] Spencer, A.J.M. (1984). *Continuum Theory of The Mechanics of Fiber-Reinforced Composites*, Springer Verlag.

[30] Swan, C.C. and Cakmak, A.S. (1994). "A hardening orthotropic plasticity model for pressure insensitive composites: continuum formulation and integration algorithm," *International Journal for Numerical Methods in Engineering*, 37: 839-860.

[31] Swan, C.C. and Kosaka, I. (1997). "Homogenization-based analysis and design of composites," *Computers and Structures*, 64: 603-621.

[32] Swan, C.C. (2007). Web-videos of a virtual full-body mannequin for clothing simulations, and the walking pants simulations are available at http://www.engineering.uiowa.edu/~swan/clothing

[33] Terzopoulos, D., Platt, J., Barr, A. and Fleischer, K. (1987). "Elastically deformable models," *Computer Graphics* (*Proc. SIGGRAPH*), 21(4): 205-214.

[34] Terzopoulos, D. and Fleischer, K. (1988). "Modeling inelastic deformation: viscoelasticity, plasticity, fracture," *Computer Graphics*, 22(4): 269-278.

[35] Carpenter, N.J., Taylor, R.L. and Katona, M.G. (1991). "Lagrange constraints for transient finite element surface contact," *International Journal for Numerical Methods in Engineering*, 32: 103-128.

[36] Belytschko, T. and Neal, M.O. (1991). "Contact-impact by the pinball algorithm with penalty and Lagrangian methods," *International Journal for Numerical Methods in Engineering*, 31: 547-572.

[37] Wriggers, P. and Simo, J.C. (1985). "A note on tangent stiffness for fully nonlinear contact problems," *Communications in Applied Numerical Methods*, 1: 199-203.

AUTHORS' ADDRESSES

Colby C. Swan, Ph.D.
University of Iowa
Civil-Environmental Engineering
4120 Seamans Center
Iowa City, Iowa 52242-1527
USA

Xiaolin Man
University of Iowa
111 Engineering Research Facility
Iowa City, Iowa 52242
USA